A Novel Safety-Oriented Control Strategy for Manipulators Based on the Observation and Adjustment of the External Momentum

Jian Liu, Yoji Yamada, Yasuhiro Akiyama, Shogo Okamoto, Yumena Iki
Graduate School of Engineering
Nagoya University
Nagoya, Japan
e-mail: liu.jian@k.mbox.nagoya-u.ac.jp

2021 International Conference on Computer, Control and Robotics (ICCCR) | 978-1-7281-9035-8/20/$31.00 ©2021 IEEE | DOI: 10.1109/ICCCR49711.2021.9349377

***Abstract*—Human safety assurance in physical human-robot interactions (pHRIs) has become a challenge for current robotic applications. Considering the safety assurance of a pHRI validation experiment, the viscoelastic properties of a human body part were investigated in a previous study and were added in a pHRI simulation. This study focuses on a threshold momentum value as an injury criterion for momentum control strategy design. A novel safety-oriented control strategy is proposed, which consists of a conventional proportional-derivative (PD) controller, an external momentum observer-based compensator for monitoring the external momentum, and an adjustment loop for shaping the trajectory motion command to bind the external momentum within the injury criterion. The proposed control strategy can be designed without needing to obtain the mechanical properties of the environment. The strategy can also be combined with the related injury criterion. In addition, it shows the effectiveness of ensuring safety even in the worst pHRI clamping situation, where a human body part can escape from such a situation. Simulation results show that the proposed control strategy performs well in the trajectory tracking task, and the adjustment loop successfully shapes the predetermined trajectory motion command to bind the external momentum within the injury criterion.**

Keywords-control strategy; safety; human-robot interaction; momentum injury criteria; viscoelasticity; in-vivo experiment

I. INTRODUCTION

As the application of robots extends to various fields, there is a strong desire to remove the guiding fence separating humans from robots [1]. Therefore, humans and robots must share the same physical environment, which inevitably increases the possibility of the physical human-robot interaction (pHRI) [2]. Ensuring human safety in the human-robot coexistence environment has been one of the control issues for the past 20 years.

The pHRI can be divided into two types: free bumping and clamping, in which the latter is the worst case and attracts more attention from researchers. The safety oriented control strategies for this problem are divided into pre- and post-contact safety strategies [3], and Yamada et al. [4] [5] first proposed a methodology for the latter, which can be summarized as establishing pain tolerances via human experiments and inserting such criteria into a control strategy for limiting the motions of the manipulator.

Several control strategies were considered to show the effectiveness and friendliness of humans in the pHRI framework, such as either uncontrolled or controlled stop (safe stop, hereafter) [6], active stiffness control, impedance control, hybrid control. The safe stop is wildly used as a general method for the motion/contact force limitation to guarantee the safety of pHRI [4] [7] [8]. The stop function is triggered when the measured or estimated external force exceeds the predetermined threshold value. The external force exists even after the manipulator stops; therefore, if the human body part is clamped by obstacles and the manipulator, it is difficult to escape from such a hazardous situation. Active stiffness control [9] [10] is part of the impedance control [11], which intends to make the manipulator softer in the pHRI task to generate a smaller contact force. However, to adjust the contact force, the mechanical properties of the human body part must be taken into account when optimizing the stiffness parameter [12] [13]. The hybrid control [14] [15] can realize different control modes in one direction of a specified coordinate (generally, the Cartesian coordinate); therefore, for safety considerations, the control mode switching from motion to force control should be triggered when the contact force is detected, which may result in reaction time and instability problems. Other strategies focus on reducing the reference torque input; for example, if a collision is detected, the torque input will be changed into only a gravity compensator [16], which means that a collision occurs due to the remaining kinematic energy and the contact force for stopping the manipulator increases.

The foregoing post-contact control strategies require the instruction of injury criteria, for example, the contact velocity/force limitation [17] or transferred energy [18]. However, for the safety of pHRI, it is necessary to take into account not only the contact velocity v_c of the impactor but also its mass because they are associated directly with the impulse resulting in contact force. The momentum equals the mass multiplied by the velocity or integral of the contact force. It is expected to establish a bridge of motion and force variables in the control strategy as well as for the parameter to comply with the injury criteria. The momentum injury criterion L_{index} can be obtained by a simple transformation from the accepted maximum transferred energy E_{index} by taking $L_{index} = 2E_{index}/v_c$. It is almost constant as shown in the

result of the study [7]. Haddadin et al. [19] studied the injury criterion associated with mass and velocity values obtained through collision experiments, and L_{index} was seen to be a function of the velocity or the mass.

From the above consideration, this study aims to establish a control strategy of a collaborative manipulator taking into account the momentum as a directly adjustable signal [20]. Sensors attached to the end effector are generally used for force measurements and monitoring the contact force. However, if the contact part of the manipulator is not the end effector but some parts of the links of the manipulator, the mechanism to guarantee safety will lose efficacy [21] [22]. Therefore, a second-order external momentum observer is proposed for estimating and monitoring the external momentum generated in contact.

The external momentum estimated by the second-order observer is fed to the main control loop to give zero compliance to the entire control structure. Based on the observer, an adjustment loop converts the momentum signal into the motion signal for reshaping the motion trajectory command when the external momentum exceeds the injury criterion in the pHRI. In this study, a novel safety-oriented control strategy is proposed consisting of a conventional proportional-derivative (PD) controller, an external momentum observer-based compensator, and an adjustment loop, with the following advantages:

- Operability of the injury-related variable: the external/contact momentum can be bounded in a desired safe zone;
- Effectiveness for the worst case: The human body part can escape from the clamping situation;
- Intercommunity: It is common to all (if any) related control strategies;
- It does not require any prior information about the mechanical properties of the environment (the human body parts);
- Also friendly to such environments as rigid obstacles, by which contact takes and achieved.

The reminder of this paper is organized as follows. Section II introduces the mathematical model of the proposed control strategy. Section III presents the in-vivo experiment obtaining the viscoelasticity of the human upper arm, and the simulation results regarding the operational space control to demonstrate the effectiveness of the proposed momentum adjustment method. The conclusion is discussed in Section IV.

II. SAFETY-ORIENTED CONTROL STRATEGY

The momentum controller proposed in the study [23] deals with the Cartesian force control of the manipulator for both the stability at the singularity and the applicability in the dynamic state. In this study on the safety-oriented control strategy based on the momentum injury criteria, we found that the momentum controller is more suitable for interpreting its mechanism and functionality, so the momentum controller dealing with the Cartesian motion is introduced here as an element of our proposed safety-oriented control strategy.

A. Introduction of the Momentum Controller

The dynamic model of an n-DOF manipulator is expressed by

$$\boldsymbol{M}(\boldsymbol{\theta})\ddot{\boldsymbol{\theta}}+\boldsymbol{C}\left(\boldsymbol{\theta},\dot{\boldsymbol{\theta}}\right)\dot{\boldsymbol{\theta}}+\boldsymbol{G}(\boldsymbol{\theta})=\boldsymbol{\tau} \tag{1}$$

where $\boldsymbol{M}(\boldsymbol{\theta}),\boldsymbol{C}\left(\boldsymbol{\theta},\dot{\boldsymbol{\theta}}\right)\in\mathcal{R}^{n\times n}$ denotes the inertia and the Coriolis/Centripetal matrices, $\boldsymbol{G}(\boldsymbol{\theta})\in\mathcal{R}^{n}$ the gravity vector, $\boldsymbol{\theta}\in\mathcal{R}^{n}$ the vector of joint variables, and $\boldsymbol{\tau}\in\mathcal{R}^{n}$ the net torque for operating the manipulator.

The traditional computed torque control in the operational space for an n-DOF manipulator employs the inverse dynamic model for transforming a given command motion trajectory of the operational space into that of the joint space and a PD or proportional-integral-derivative (PID) controller with an adjustment loop to compensate the Coriolis/Centripetal term $\boldsymbol{C}\left(\boldsymbol{\theta},\dot{\boldsymbol{\theta}}\right)\dot{\boldsymbol{\theta}}$ and the gravity term $\boldsymbol{G}(\boldsymbol{\theta})$ considering the linearization of the dynamic model (1) [24] or directly combining the command motion. The motion trajectory of the operational space is input into the controller loop by using the inverse of the Jacobian matrix [25].

Ohnishi et al. [23] proposed a momentum controller for the operational-space motion tracking task, which can avoid the calculation of the inverse of the Jacobian matrix $\boldsymbol{J}$. The reference torque signal for the manipulator is set as

$$\boldsymbol{\tau}_{ref}=\frac{d}{dt}\left(\boldsymbol{J}^{T}\bar{\boldsymbol{M}}\int\ddot{\boldsymbol{x}}_{ref}dt\right) \tag{2}$$

$$\dot{\boldsymbol{x}}=\boldsymbol{J}\dot{\boldsymbol{\theta}} \tag{3}$$

where $\ddot{\boldsymbol{x}}_{ref},\dot{\boldsymbol{x}}\in\mathcal{R}^{m}$ denotes the reference operational acceleration signal and the actual velocity in operational space, and m is the degree of freedom of the operational space.

The momentum controller is shown in Fig. 1. The reference signal $\ddot{\boldsymbol{x}}_{ref}$ is converted first into an operational-space momentum $\bar{\boldsymbol{M}}\dot{\boldsymbol{x}}_{ref}$, joint-space momentum $\boldsymbol{M}\dot{\boldsymbol{\theta}}_{ref}$, and then torque $\boldsymbol{\tau}_{ref}$ in sequence, which can also be classified as the computed torque control. The controller $C(s)$ can be similar to a conventional controllers such as the PD or PID controller,

$$\ddot{\boldsymbol{x}}_{ref}=\boldsymbol{K}_{p}\boldsymbol{e}_{x}+\boldsymbol{K}_{d}\dot{\boldsymbol{e}}_{x}+\ddot{\boldsymbol{x}}_{d} \tag{4}$$

$$\boldsymbol{e}_{x}=\boldsymbol{x}_{d}-\boldsymbol{x} \tag{5}$$

where $\boldsymbol{K}_{p},\boldsymbol{K}_{d}\in\mathcal{R}^{m\times m}$ denotes the gain matrices for the PD controller, $\boldsymbol{x}_{d},\boldsymbol{x}\in\mathcal{R}^{m}$ the operational-space command motion trajectory of the end effector and the actual one.

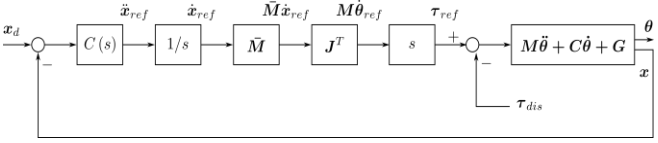

Figure 1. " Momentum controller.

Since the conversion from the operational-space momentum into the joint-space one requires the transpose of the Jacobian matrix $\boldsymbol{J}^T$ but not the inverse of it $\boldsymbol{J}^{-1}$, this control strategy performs well under the situation that the manipulator passes through the singularity point and is convenient for the controller loop calculation. On the other hand, the momentum controller provides a more intuitive way of obtaining the reference torque signal for commanding the manipulator. This study employs a momentum controller for the convenience of handling momentum signals and combining them with momentum injury criteria.

B. Compensator for the Momentum Controller

A compensator is necessary for eliminating the gravity and Coriolis/centrifugal terms as well as maintaining the stability of the PD controller.

The kinetic energy of an n-DOF manipulator is

$$\mathcal{K} = \frac{1}{2}\dot{\boldsymbol{\theta}}^T \boldsymbol{M}\dot{\boldsymbol{\theta}} = \frac{1}{2}\dot{\boldsymbol{x}}^T \bar{\boldsymbol{M}}\dot{\boldsymbol{x}} \tag{6}$$

where $\mathcal{K} \in \mathcal{R}$ denotes the kinetic energy, and $\bar{\boldsymbol{M}} \in \mathcal{R}^{m\times m}$ is the inertia matrix in the operational space.

Corresponding to Lagrange's formula, the dynamics in the joint space of the manipulator is

$$\frac{d}{dt}\left(\boldsymbol{M}\dot{\boldsymbol{\theta}}\right) - \frac{\partial \mathcal{K}}{\partial \boldsymbol{\theta}} + \frac{\partial \mathcal{U}}{\partial \boldsymbol{\theta}} = \boldsymbol{\tau} = \boldsymbol{\tau}_{ref} + \boldsymbol{\tau}_{ext} + \boldsymbol{\tau}_{dis} \tag{7}$$

where $\boldsymbol{\tau}_{ext}$ denotes the torque corresponding to the external force, $\boldsymbol{\tau}_{dis}$ the disturbance torque, $\mathcal{U} \in \mathcal{R}$ the potential energy. Note that $\partial \mathcal{U}/\partial \boldsymbol{\theta} = \boldsymbol{G}(\boldsymbol{\theta})$, and $\partial(\cdot)/\partial \boldsymbol{\theta} = \boldsymbol{J}^T\left[\partial(\cdot)/\partial \boldsymbol{x}\right]$.

Introducing the Jacobian matrix to connect the joint and operational space,

$$\boldsymbol{M}\dot{\boldsymbol{\theta}} = \boldsymbol{J}^T \bar{\boldsymbol{M}}\dot{\boldsymbol{x}} \tag{8}$$

(2), (7) and (8) can be combined as

$$\begin{aligned} \boldsymbol{J}^T \bar{\boldsymbol{M}}\dot{\boldsymbol{x}}_{ref} = \boldsymbol{J}^T \bar{\boldsymbol{M}}\dot{\boldsymbol{x}} - \int \frac{\partial \mathcal{K}}{\partial \boldsymbol{\theta}} dt + \int \frac{\partial \mathcal{U}}{\partial \boldsymbol{\theta}} dt \\ - \int \boldsymbol{\tau}_{ext} dt - \int \boldsymbol{\tau}_{dis} dt \end{aligned} \tag{9}$$

A compensator C_{ff} can be proposed to eliminate the effect of the terms in the right hand side of (9),

$$C_{ff} = -\frac{\partial \mathcal{K}}{\partial \boldsymbol{\theta}} + \boldsymbol{G}(\boldsymbol{\theta}) - \boldsymbol{\tau}_{dis} \tag{10}$$

Which can be added to $\boldsymbol{\tau}_{ref}$. Consequently, (9) becomes

$$\bar{\boldsymbol{M}}\dot{\boldsymbol{x}}_{ref} = \bar{\boldsymbol{M}}\dot{\boldsymbol{x}} - \boldsymbol{J}^{-T}\int \boldsymbol{\tau}_{ext} dt \tag{11}$$

Corresponding to the study [23], the Jacobian matrix $\boldsymbol{J}$ can be regarded as a constant matrix in some cases of slow movements, and (11) becomes

$$\bar{\boldsymbol{M}}\dot{\boldsymbol{x}}_{ref} = \bar{\boldsymbol{M}}\dot{\boldsymbol{x}} - \int \boldsymbol{F}_{ext} dt \tag{12}$$

The compensator is shown at the bottom of Fig. 2.

C. External Momentum Observer

To estimate the external momentum, that is, the integral of the external force, a traditional way is to estimate the external force by utilizing observers or comparing the response torque from (1) with the reference torque signal from the controller, and taking integral operator. However, in a momentum controller, the reference signals contain a momentum signal, which provides a more convenient way. A second-order observer is proposed as

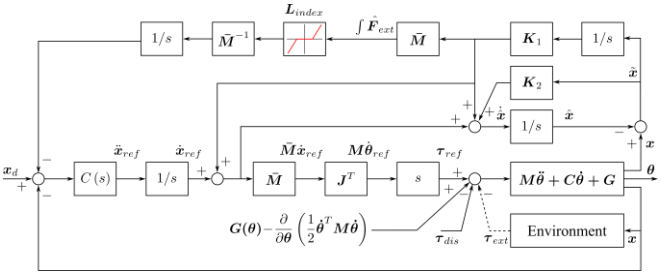

Figure 2. " Proposed safety-oriented control strategy for the operational-space task.

$$\dot{\hat{\boldsymbol{x}}} = \dot{\boldsymbol{x}}_{ref} + \boldsymbol{K}_2\tilde{\boldsymbol{x}} + \boldsymbol{K}_1\int \tilde{\boldsymbol{x}} dt \tag{13}$$

$$\hat{\boldsymbol{x}} = \int \dot{\hat{\boldsymbol{x}}} dt + \boldsymbol{x}(0) \tag{14}$$

$$\hat{\boldsymbol{L}}_{ext} = \hat{\boldsymbol{F}}_{ext} dt = \bar{\boldsymbol{M}}\boldsymbol{K}_1 \int \tilde{\boldsymbol{x}} dt \tag{15}$$

where $\boldsymbol{K}_2, \boldsymbol{K}_1 \in \mathcal{R}^{m\times m}$ are positive definite gain matrices, and $\tilde{\boldsymbol{x}} = \boldsymbol{x} - \hat{\boldsymbol{x}}$. Equations (13) to (15) are shown in the top right part of Fig. 2.

The relation between the estimated external momentum and the actual one is

$$\hat{\boldsymbol{L}}_{ext} = \boldsymbol{K}_1\left(s^2\boldsymbol{I} + s\boldsymbol{K}_2 + \boldsymbol{K}_1\right)^{-1}\boldsymbol{L}_{ext} \tag{16}$$

if $\boldsymbol{K}_1$ and $\boldsymbol{K}_2$ are the diagonal matrices.

The error dynamics of the estimated external momentum is

$$\tilde{\boldsymbol{L}}_{ext} = s\left(s\boldsymbol{I} + \boldsymbol{K}_2\right)\left(s^2\boldsymbol{I} + s\boldsymbol{K}_2 + \boldsymbol{K}_1\right)^{-1}\boldsymbol{L}_{ext} \tag{17}$$

where $\tilde{\boldsymbol{L}}_{ext} = \boldsymbol{L}_{ext} - \hat{\boldsymbol{L}}_{ext}$. The momentum estimation error converges to zero for a constant external momentum. For a constant external force, $\boldsymbol{L}_{ext} = \boldsymbol{F}_{ext}/s^2$ leads the estimation error to converge to $\boldsymbol{K}_2\boldsymbol{K}_1^{-1}\boldsymbol{F}_{ext}$. This requires the gain matrix $\boldsymbol{K}_1$ to be as large as enough.

D. Adjustment loop

Unlike the active stiffness control [9], the estimated external momentum $\hat{\boldsymbol{L}}_{ext}$ can be compared with the momentum injury criteria $\boldsymbol{L}_{index}$. If $\hat{\boldsymbol{L}}_{ext}$ exceeds $\boldsymbol{L}_{index}$, an adjustment loop will be triggered to adjust the command motion trajectory via the mass matrix $\bar{\boldsymbol{M}}$ as follows:

$$\boldsymbol{x}_{adj} = \begin{cases} 0, & \hat{\boldsymbol{L}}_{ext} \le \boldsymbol{L}_{index} \\ \int \bar{\boldsymbol{M}}^{-1}\hat{\boldsymbol{L}}_{ext} dt, & \hat{\boldsymbol{L}}_{ext} > \boldsymbol{L}_{index} \end{cases} \tag{18}$$

Equations (4), (5) are modified as follows:

$$\ddot{\boldsymbol{x}}_{ref} = \boldsymbol{K}_p\boldsymbol{e}_x + \boldsymbol{K}_d\dot{\boldsymbol{e}}_x + \ddot{\boldsymbol{x}}_d - \ddot{\boldsymbol{x}}_{adj} \tag{19}$$

$$\boldsymbol{e}_x = \boldsymbol{x}_d - \boldsymbol{x}_{adj} - \boldsymbol{x} \tag{20}$$

From (18) and (19), it is seen that the momentum variable manipulated in the adjustment loop provides a more intuitive and essential transformation between the force and

motion variables. The adjustment loop can eliminate the external force because the integral of the external force is manipulated within the injury criterion only if the external force decreases to zero. On the other hand, the proposed method does not require the mechanical properties of the environment.

III. SIMULATION

A. *Viscoelasticity of Human Upper Arm*

The viscoelasticity of the human upper arm was estimated by human experiments and input in the simulation to complete the pHRI task. Our previous study [26] focused on modeling the viscoelasticity of the soft tissue on human hands, inherited from which a nonlinear 5-element viscoelastic model (Fig. 3(a)) is taken into account for modeling the mechanical property of the human upper arm. The in-vivo experimental design is shown in Fig. 4. The impactor was moved by the manipulator at a velocity of 250 mm/s to contact the human upper arm and stopped if the compression displacement reached 32 mm. The maximum compression displacement was carefully determined in advance by communicating with human subjects by increasing the compression displacement gradually until they felt uncomfortable. In addition, the safety device uses a release mechanism to ensure the safety of human subjects. The support plant for the human upper arm is fixed on a slide and is attracted by two magnets, so the upper arm can avoid contact if the contact force exceeds the attractive force (100 N according to the study [7]) provided by magnets. The experiment was conducted with the approval of the Ethics Committee of the Department of Engineering, Nagoya University.

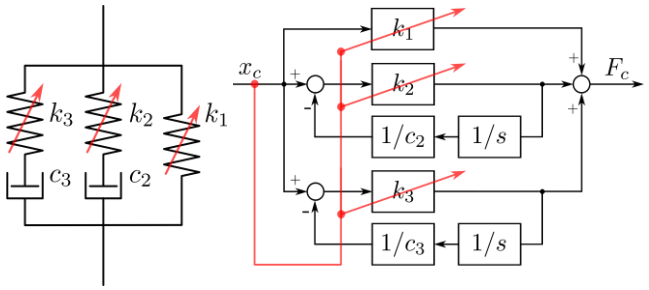

Figure 3. " Nonlinear 5-element viscoelastic model and its block diagram.

The mathematical expression of the 5-element viscoelastic model is

$$x_c = \begin{cases} v_c t, & 0 \le t < t_p \\ v_c t_p, & t \ge t_p \end{cases} \tag{21}$$

$$F_c = \begin{cases} k_1 v_c t + \sum_{i=2}^{3} c_i v_c \left(1 - e^{-\frac{k_i}{c_i} t}\right), & 0 \le t < t_p \\ k_1 v_c t_p + \sum_{i=2}^{3} c_i v_c \left(1 - e^{-\frac{k_i}{c_i} t_p}\right) e^{-\frac{k_i}{c_i}(t - t_p)}, & t \ge t_p \end{cases} \tag{22}$$

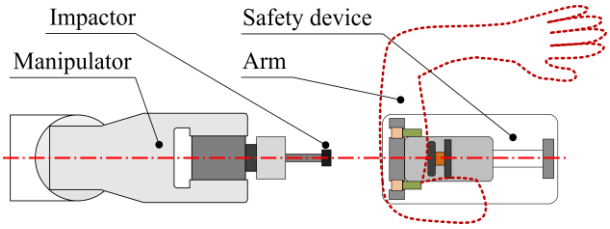

Figure 4. " Aerial view of the experimental apparatus.

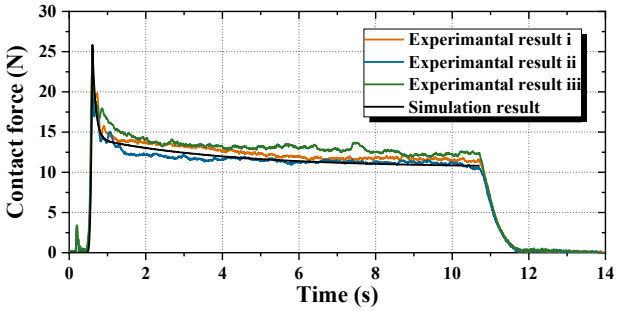

Figure 5. " Comparison between the experimental and simulation results.

where x_c yields the compression displacement, v_c contact velocity, t_p peak value time, F_c contact force, k_i and c_i stiffness of spring and damping ratio of the damper, as shown in Fig. 3(a).

Note that k_i has a nonlinear relationship with the compression displacement x_c. A coefficient γ_i is introduced to describe the nonlinearity:

$$k_1 = \gamma_1 x_c^2 \tag{23}$$

$$k_2 = \gamma_2 x_c^3 \tag{24}$$

$$k_3 = \gamma_3 x_c^3 \tag{25}$$

With (21)-(25), a set of viscoelastic parameters is obtained by curve fitting, as shown in Table I, and by using the block diagram of the nonlinear model shown in Fig. 3(b), the simulation result is obtained and shown in Fig. 5. This nonlinear model is intended to be used in human-robot contact simulation as a substitute for the human upper arm, and note that it is not to be applied for controller design.

TABLE I. VISCOELASTIC PARAMETERS OF THE HUMAN UPPER ARM

Parameters	γ_1	γ_2	γ_3	c_2	c_3
Value[a]	3.11×10^{-4}	3.27×10^{-6}	1.48×10^{-5}	0.3934	0.0415
Unit	N/mm^3			N/(mm/s)	

a. Experimental condition: 32 mm compression displacement and 250 mm/s contact velocity.

TABLE II. STRUCTURE PARAMETERS OF THE 2-DOF MANIPULATOR

Parameters	l_1	l_2	m_1	m_2	g
Value	0.160	0.210	1.580	0.970	9.807
Unit	m	m	kg	kg	m/s^2

B. *Parameter Settings for Simulation*

Using the Simulink® simulation platform, a simple 2-DOF manipulator was established, as shown in Fig. 6(a). The structure parameters of this 2-DOF manipulator are shown in Table II. In such a case, a conventional PD controller with a gravity compensator performs well in a non-external force environment [27].

In addition, the viscoelastic model of the human upper arm mentioned in section III-A was established in the simulation by a linear joint attached to two mass units. The viscoelastic parameters were set as shown in Table I, and the distance between the contact surface of the viscoelastic model and the base of the manipulator is set as 250 mm, as shown in Fig. 6(b).

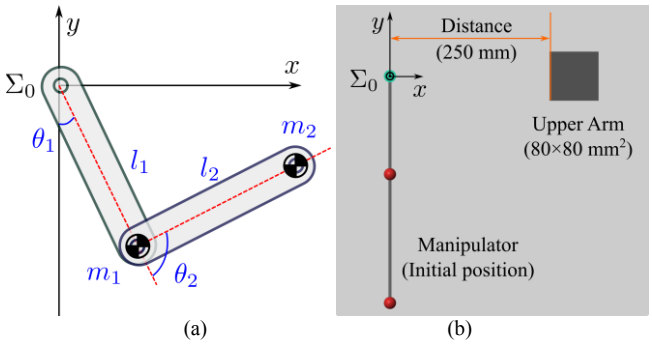

Figure 6. " Simulation models of the 2-DOF manipulator and upper arm.

For the differential operator in (2), a pseudo-differential operator or a high-pass filter is used,

$$s = g_c s / (g_c + s) \tag{26}$$

where $g_c/(2\pi)$ is the cutoff frequency.

The mass matrix $\bar{\boldsymbol{M}}$ is calculated as (27) when the manipulator is near the singularity,

$$\bar{\boldsymbol{M}} = \begin{cases} \left(\boldsymbol{J}\boldsymbol{M}^{-1}\boldsymbol{J}^T + \left(\alpha - \det\left\{\boldsymbol{J}\boldsymbol{M}^{-1}\boldsymbol{J}^T\right\}\right)\begin{bmatrix} 0 & 0 \\ 0 & 1 \end{bmatrix} \right)^{-1}, & \\ & \det\left\{\boldsymbol{J}\boldsymbol{M}^{-1}\boldsymbol{J}^T\right\} < \alpha \\ \left(\boldsymbol{J}\boldsymbol{M}^{-1}\boldsymbol{J}^T\right)^{-1}, & \det\left\{\boldsymbol{J}\boldsymbol{M}^{-1}\boldsymbol{J}^T\right\} \geq \alpha \end{cases} \tag{27}$$

In the simulation, $\boldsymbol{K}_p$, $\boldsymbol{K}_d$, $\boldsymbol{K}_1$ and $\boldsymbol{K}_2$ are set as $1600\boldsymbol{I}_2$, $80\boldsymbol{I}_2$, $400\boldsymbol{I}_2$ and $40\boldsymbol{I}_2$, respectively, g_c as 100, α as 0.0645 and $\boldsymbol{L}_{index}$ as $\begin{bmatrix} 10 & 10 \end{bmatrix}^T$. $\boldsymbol{I}_2$ is a 2-by-2 identify matrix.

The motion commands for the robot are listed in Table III. M-I is used to test the performance at the singularity point and keep away from it, M-II for testing the performance in the non-contact case, and M-III for the impacting.

C. *Discussion*

The results of the simulation without the compensator are shown in Fig. 7(a), from which it can be seen that the manipulator performs well in tracking the command signal in the non-contact period (0 to 10.4 s), even at the initial phase of motion where the manipulator is located at a singularity point. In the contact period, the x-direction tracking error remains small and does not converge to zero caused by the PD controller with no integral terms eliminating the steady-state error. Nevertheless, the observed external momentum is fed to the reference signal $\bar{\boldsymbol{M}}\dot{\boldsymbol{x}}_{ref}$ as an external momentum compensator. The steady-state error is then eliminated without changing the estimated external momentum, as shown in Fig. 7(d).

TABLE III. MOTION COMMAND FOR THE 2-DOF MANIPULATOR

Name	Motion[a]	Time period
Motion I (M-I)	(0, -370) to (30, -298)	0 to1 s
	Stop	1 to 3 s
Motion II (M-II)	(30, -298) to (150, 0)	3 to 7 s
	Stop	7 to 10 s
Motion III (M-III)	(150, 0) to (282.4, 0)	250 mm/s
	Stop and end	to 20 s

a. Unit: mm.

Comparing the external momentum values in Fig. 7(b) with those in Fig. 7(e), the adjustment loop affects both the estimated external momentum $\hat{\boldsymbol{L}}_{ext}$ and the actual one $\boldsymbol{L}_{ext}$, which are suppressed within the injury criterion $\boldsymbol{L}_{index}$, and the external force $\boldsymbol{F}_{ext}$ rises as shown in Fig. 7(f) when $\hat{\boldsymbol{L}}_{ext} \leq \boldsymbol{L}_{index}$. However, it quickly decreases to 0 for satisfying $\hat{\boldsymbol{L}}_{ext} \leq \boldsymbol{L}_{index}$. The adjustment loop shows a good performance for limiting the external momentum and eliminating the contact force in the pHRI task. Moreover, the design of the adjustment loops uses only the mass matrix of the manipulator that can be effortlessly obtained by numerical computation and does not have to model the mechanical properties of the environment (such as the human body part). It can be inferred that, if the human body part is clamped in the working environment between the end effector of the manipulator and some obstacles (e.g., work table), it can escape from such clamping situations by directly moving the end effect against the contact direction to enlarge the distance between the end effector and the obstacle.

IV. CONCLUSION

This study proposes a novel safety-oriented control strategy consisting of a conventional PD controller, an external momentum observer-based compensator, and an adjustment loop. The proposed control strategy can be designed without the necessity of obtaining the mechanical properties of the environment and can combine the related injury variable. It effectively ensures the safety in the clamping situation since the momentum variable manipulated by the adjustment loop processes more intuition and essence of transform between force and motion variables.

The proposed control strategy was verified by simulations of the worst-case scenario in which a 2-DOF

manipulator was operated to accomplish an operational-space task while the human soft tissue was clamped. The results showed that the observer-based compensator performed well in the trajectory tracking task, and the adjustment loop successfully reshaped the predetermined trajectory motion command to bind the external momentum within the injury criterion. Therefore, it is inferred that the human body part can escape from the clamping situation.

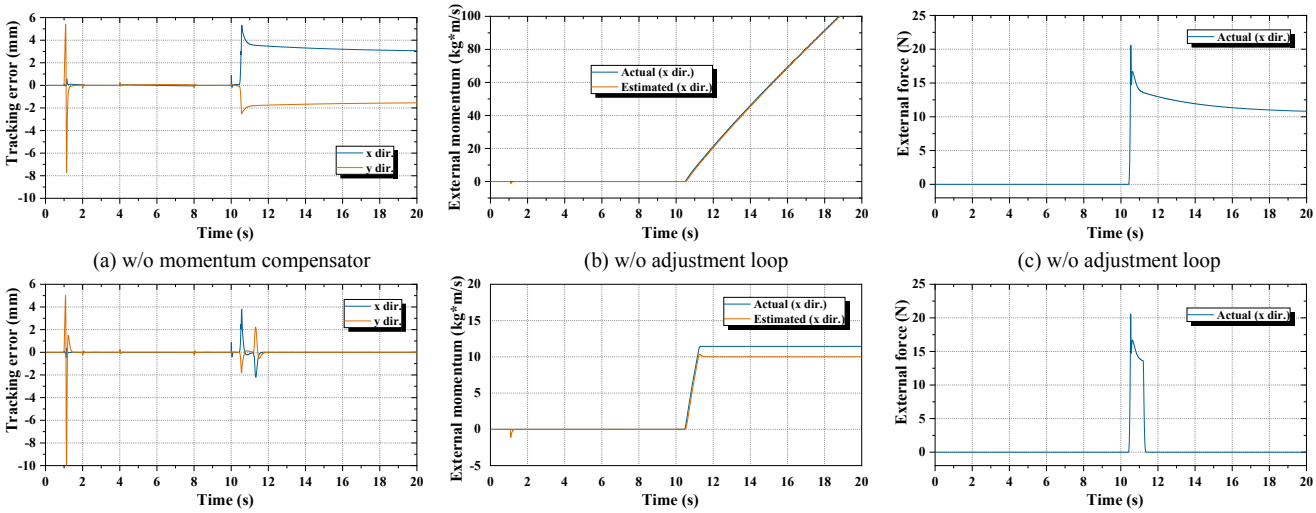

(a) w/o momentum compensator (b) w/o adjustment loop (c) w/o adjustment loop

(d) w/ adjustment loop (e) w/ adjustment loop (f) w/ adjustment loop

Figure 7. " Simulation results.

ACKNOWLEDGMENT

This study was financially supported by "Knowledge Hub Aichi" research project: R7 and conducted through "Construction of Risk Assessment System for Service Robot Applications: Establishment of a V&V Testing Method".

REFERENCES

[1] T. Ogure, Y. Nakabo, S. Jeong, and Y. Yamada, "Hazard analysis of an industrial upper-body humanoid," Ind. Rob., vol. 36, no. 5, pp. 469–476, 2009, doi: 10.1108/01439910910980196.

[2] B. Siciliano and O. Khatib, *Springer handbook of robotics*, vol. 46, no. 06. 2009.

[3] J. Xia, Z. Jiang, H. Liu, H. Cai, and G. Wu, "A Novel hybrid safety-control strategy for a manipulator," Int. J. Adv. Robot. Syst., vol. 11, no. 1, pp. 1–10, 2014, doi: 10.5772/58316.

[4] Y. Yamada, Y. Hirasawa, S. Y. Huang, and Y. Umetani, "Fail-safe human/robot contact in the safety space," in *Proceedings 5th IEEE International Workshop on Robot and Human Communication. RO-MAN'96 TSUKUBA*, 1996, pp. 59–64, doi: 10.1109/roman.1996.568748.

[5] K. Suita, Y. Yamada, N. Tsuchida, K. Imai, H. Ikeda, and N. Sugimoto, "Failure-to-safety 'Kyozon' system with simple contact detection and stop capabilities for safe human-autonomous robot coexistence," in *Proceedings - IEEE International Conference on Robotics and Automation*, 1995, vol. 3, pp. 3089–3096, doi: 10.1109/robot.1995.525724.

[6] IEC, *60204-5.1: Safety of machinery-Electrical equipment of machines-Part 1: General requirements*. 2009.

[7] "Robots and robotic devices — Collaborative robots," Iso/Ts 15066, vol. 2016, pp. 1–33, 2016.

[8] S. Haddadin, A. Albu-Schäffer, A. Albu-Schaffer, and A. Albu-sch, "Evaluation of collision detection and reaction for a human-friendly robot on biological tissues," 6th IARP/IEEE-RAS/EURON Work. Tech. Challenges Dependable Robot. Hum. Environ., 2008, [Online]. Available: http://www.phriends.eu/Stanford_08a.pdf.

[9] J. K. Salisbury, "Active Stiffness Control of a Manipulator in Cartesian Coordinates.," in *Proceedings of the IEEE Conference on Decision and Control*, 1980, vol. 1, pp. 95–100, doi: 10.1109/cdc.1980.272026.

[10] A. Ajoudani, N. G. Tsagarakis, and A. Bicchi, "On the role of robot configuration in Cartesian stiffness control," in *Proceedings - IEEE International Conference on Robotics and Automation*, 2015, vol. 2015-June, no. June, pp. 1010–1016, doi: 10.1109/ICRA.2015.7139300.

[11] N. Hogan, "Impedance Control: An Approach to Manipulation," in *1984 American Control Conference*, Jul. 1984, pp. 304–313, doi: 10.23919/ACC.1984.4788393.

[12] S. Morinaga and K. Kosuge, "Collision detection system for manipulator based on adaptive impedance control law," in *2003 IEEE International Conference on Robotics and Automation (Cat. No.03CH37422)*, 2003, vol. 1, pp. 1080–1085, doi: 10.1109/ROBOT.2003.1241736.

[13] C. C. Cheah and D. Wang, "Learning impedance control for robotic manipulators," IEEE Trans. Robot. Autom., vol. 14, no. 3, pp. 452–465, 1998, doi: 10.1109/70.678454.

[14] M. H. Raibert and J. J. Craig, "Hybrid position/force control of manipulators," J. Dyn. Syst. Meas. Control. Trans. ASME, vol. 103, no. 2, pp. 126–133, 1981, doi: 10.1115/1.3139652.

[15] A. De Luca and R. Mattone, "Sensorless robot collision detection and hybrid force/motion control," in *Proceedings - IEEE International Conference on Robotics and Automation*, 2005, vol. 2005, no. April, pp. 999–1004, doi: 10.1109/ROBOT.2005.1570247.

[16] S. Haddadin, A. Albu-Schäffer, A. De Luca, and G. Hirzinger, "Collision detection and reaction: A contribution to safe physical human-robot interaction," in *2008 IEEE/RSJ International Conference on Intelligent Robots and Systems, IROS*, 2008, pp. 3356–3363, doi: 10.1109/IROS.2008.4650764.

[17] S. Haddadin, *Towards safe robots: approaching Asimov's 1st law*, vol. 90. 2014.

[18] T. Fujikawa, R. Sugiura, R. Nishikata, and T. Nishimoto, "Critical contact pressure and transferred energy for soft tissue injury by blunt impact in human-robot interaction," in *International Conference on*

Control, Automation and Systems, 2017, vol. 2017-Octob, pp. 867–872, doi: 10.23919/ICCAS.2017.8204347.

[19] S. Haddadin *et al.*, "On making robots understand safety: Embedding injury knowledge into control," Int. J. Rob. Res., vol. 31, no. 13, pp. 1578–1602, 2012, doi: 10.1177/0278364912462256.

[20] S. Sakaino and K. Ohnishi, "Dynamic force control having no singular point on momentum control system," in *Proceedings of the 2007 4th IEEE International Conference on Mechatronics, ICM 2007*, 2007, no. May, pp. 8–10, doi: 10.1109/ICMECH.2007.4280048.

[21] A. Alcocer, A. Robertsson, A. Valera, and R. Johansson, "Force estimation and control in robot manipulators," IFAC Proc. Vol., vol. 36, no. 17, pp. 55–60, 2003, doi: 10.1016/s1474-6670(17)33369-4.

[22] K. Ohishi, M. Miyazaki, M. Fujita, and Y. Ogino, "H/sup infinity / observer based force control without force sensor," in *Proceedings IECON '91: 1991 International Conference on Industrial Electronics, Control and Instrumentation*, 1991, vol. 2, no. 4, pp. 1049–1054, doi: 10.1109/IECON.1991.239146.

[23] S. Sakaino and K. Ohnishi, "A composition of decoupling motion controller based on momentum and its application for singular configurations," IECON Proc. (Industrial Electron. Conf., pp. 2331–2336, 2007, doi: 10.1109/IECON.2007.4460285.

[24] F. L. Lewis, D. M. Dawson, and C. T. Abdallah, *Robot Manipulator Control: Theory and Practice*. CRC Press, 2004.

[25] B. Siciliano, L. Sciavicco, L. Villani, and G. Oriolo, *Robotics: Modelling, planning and control*, no. 9781846286414. Springer Science & Business Media, 2009.

[26] Y. Iki, Y. Yamada, Y. Akiyama, S. Okamoto, K. Niwa, and J. Liu, "Evaluation of contact between a human hand and a robot end tip for designing a dummy," Proc. JSME Annu. Conf. Robot. Mechatronics, vol. 2019, no. 0, pp. 2A1-F08, 2019, doi: 10.1299/jsmermd.2019.2A1-F08.

[27] R. Kelly, "A Tuning Procedure for Stable PID Control of Robot Manipulators," Robotica, vol. 13, no. 2, pp. 141–148, 1995, doi: 10.1017/S0263574700017641.